CHAPTER ONE HUNDRED TWENTY ONE

SEDIMENT RESPONSES TO NATURAL WAVES

Alexander F. Nielsen and Angus D. Gordon*

ABSTRACT

This paper is concerned with wave-induced seabed forcing functions and sediment responses on the Australian South East Continental Shelf. The transfer of surface displacement energy to near-bed oscillatory water movement energy is examined with respect to linear and second order wave theories. Seabed sediment responses are examined by comparing field bedform size data to laboratory data with a view to determining characteristic spectral parameters that may be applied with existing theories to predict sediment responses under natural wave spectra. A rippled bed incipient motion criterion incorporating the contribution to boundary shear stress made by the presence of bedforms as well as particle size is developed empirically from field data using dimensional analysis techniques.

1. INTRODUCTION

Continental shelves are a rich source of consumables including food, minerals, oils and aggregate sands. Increasingly, they are being seen as a resource also in terms of wastes disposal, typically including dredge spoil, toxic substances and sewage. As advances in technology allow expansion in shelf resource utilisation the need to further the understanding of shelf processes increases. Of particular interest are the interactions between shelf sediments and sea bed mounted structures.

The present understanding of shelf sediment movement is based mainly on theoretical studies and laboratory experiments. While these studies have produced considerable advances in the understanding and theoretical description of sediment movement in a wave and current environment, they have mostly been carried out only for periodic, progressive, near-sinusoidal wave motions. The superposition of steady currents, where relevant, is normally based on a wholy theoretical approach. The theoretical treatment of natural wave spectra is complex and laboratory data are not readily available as random wave generators for flume and water tunnel experiments have only recently been developed.

* Coastal Branch, New South Wales Public Works Department, 140 Phillip Street, Sydney, 2000, Australia.

To meet the challenge of providing sound advice on proposed continental shelf developments off South East Australia, the application of monochromatic, theoretical and laboratory work to field conditions was studied with respect to three areas of particular interest:

- the synthesis of natural sea surface displacements and seabed water motions;
- the determination of characteristic parameters from natural wave spectra which enable the application of monochromatic theories of sediment motion to situations where finite spectral bands exist;
- the threshold of sediment movement under natural wave spectra on a rippled bed.

2. FIELD DATA

Concurrent studies off Sydney being carried out for various projects by the authors made available field data sets in 24, 60 and 80 metres water depth (Figure 1). At each site a Marsh McBirney 585 adaptive recording electromagnetic current meter was installed on the seabed in a metal frame with the sensor 1 metre above the bed. Details of the recording and calibration data are given in Gordon and Hoffman (in prep) and Nielsen (1984). Three years of data were collected at the 24 metre site while 6 months data were taken at the two deeper sites.

Two Datawell 700 mm diameter waverider buoys were used. One buoy had been operating for some 13 years in deep water off Botany Bay, 7 km south of the 80 metre site (Youll, 1981). The other was installed adjacent to the 24 metre site (Site 2, Figure 1).

Seabed surface features were mapped using an Atlas Deso 20 Fathometer and Klein side-scan sonar equipment calibrated by sediment sampling, bottom photography and diver observation (Gordon and Hoffman, 1984, and in prep.). Seabed observations at the 60 and 80 metre sites were made using a time lapse camera system synchronised with the current meter recording program. Seabed observations at the 24 metre sites were made by divers. The sediment characteristics at each site are given in Table 1.

TABLE 1

SEDIMENT GRAIN SIZE PARAMETERS

Site	Depth (m)	D16 (mm)	D50 (mm)	D84 (mm)	% Shell	% Fines
1	24	0.30	0.24	0.17	-	2
2	24	0.64	0.45	0.32	6	3
A5	24	0.36	0.32	0.25	-	2
B5	24	0.27	0.22	0.16	-	2
BON	60	0.33	0.26	0.18	26	14
MAL	80	0.35	0.21	0.15	33	32

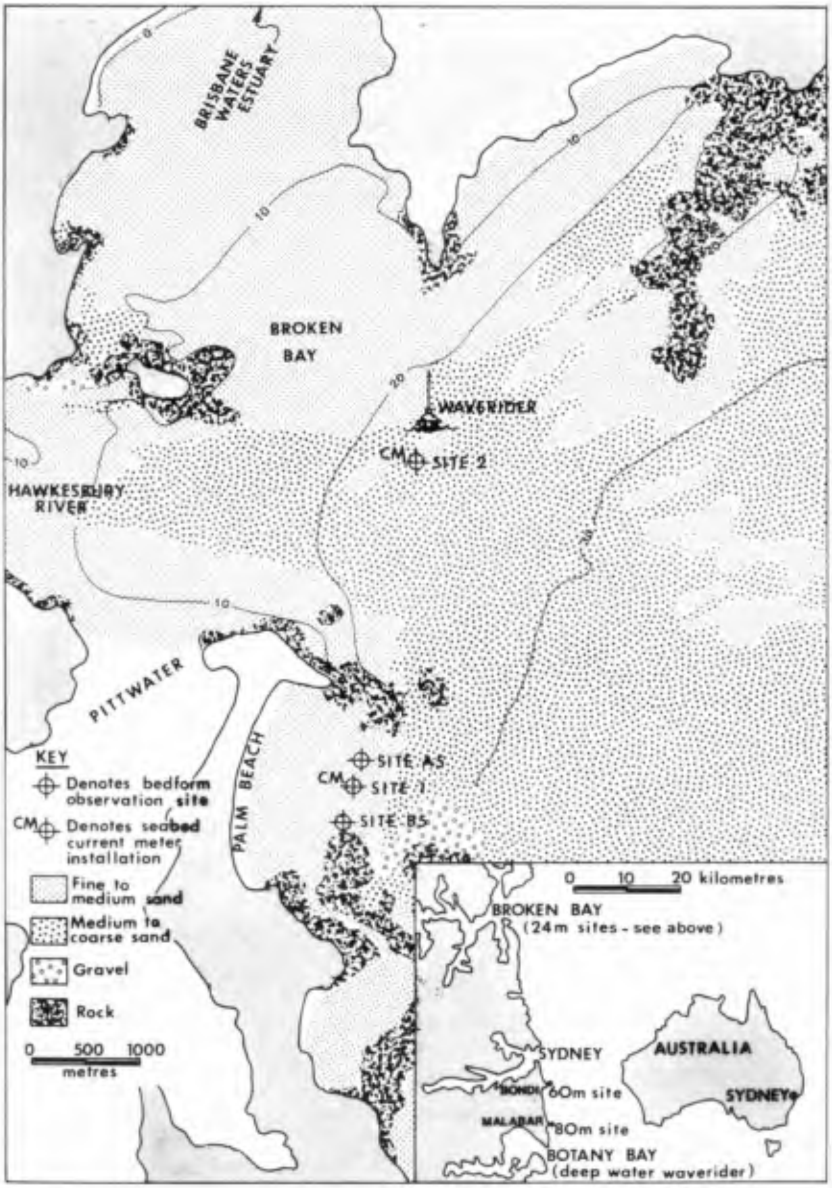

STUDY AREA
(AFTER HOFFMAN ET AL.,1980)

FIGURE 1

3. RESULTS

3.1 Synthesis of Sea Surface Displacements and Near-bed Wave-induced Water Motions

Sea surface displacement energy spectra were compared with seabed wave-induced current velocity spectra utilising wave theories to examine the modification with depth that occurs to the spectral energy distribution and to develop a technique for generating seabed spectra at sites remote from the sea surface wave data collection point.

For each waverider and current meter record a spectral energy/frequency distribution was obtained using a fast Fourier transform technique. Spectral estimates were made at 0.1 Hz frequency intervals and cross-spectral correlations were carried out at the three water depths as follows (see Nielsen (1984) for detailed discussion of these parameters):

$$\left[\frac{u}{H}\right]_f = \frac{1}{2} \cdot \left[\frac{Mc(o)}{Mw(o)}\right]^{1/2} \cdot \left[\frac{Sc(f)}{Sw(f)}\right]^{1/2} \qquad \text{Eqn. 1}$$

where:

(u)f = maximum, wave-induced, near-bed horizontal water particle velocity with period 1/f;

(H)f = wave height with period 1/f;

M(o) = is the area under the spectral energy/frequency distribution graph;

S(f) = is the normalised spectral estimate at frequency band f;

Subscript c = current meter; and

subscript w = waverider.

These empirical values were compared with theoretical computations based on both Stoke's 2nd Order and Airy theories at the 24 metre site and with Airy theory at the 60 and 80 metre sites. A typical cross-spectral correlation for a set of concurrent waverider and adjacent current meter records at the 24 m site is shown in Figure 2. Here the correlation was virtually exact compared with Stoke's 2nd Order wave theory over the frequency range encompassing most of the current energy. Some two thousand current meter records were correlated with the deepwater waverider data, and statistically analysed and compared to Airy Theory (Figure 3). In general it can be seen that Airy theory applied to the deepwater waverider data over-estimates near-bed velocities, particularly at the shallower depths. This effect at the 24 metre site is attributable to wave height attenuation through wave refraction and shoaling. Further attenuation can be attributed to friction and diffraction. These results and other factors are discussed in more detail in Gordon and Hoffman (in prep.) and Nielsen (1984).

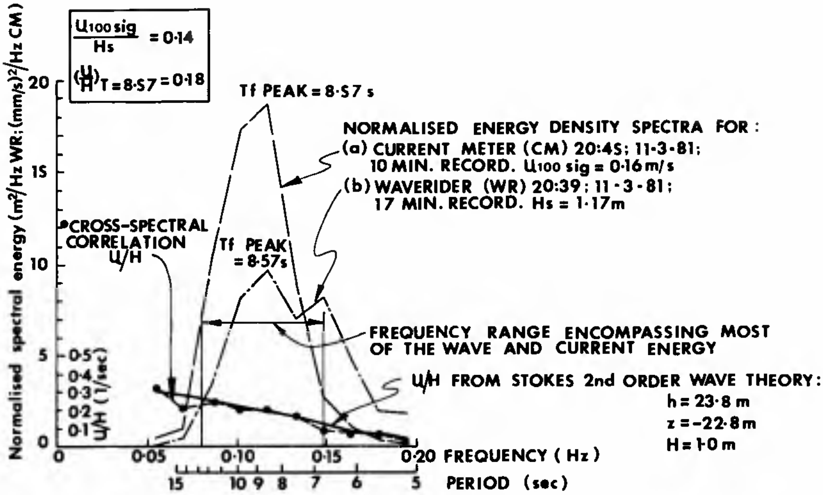

CROSS-SPECTRAL CORRELATION BETWEEN SELECTED NEARBY WAVERIDER AND CURRENT METER RECORDS

FIGURE 2

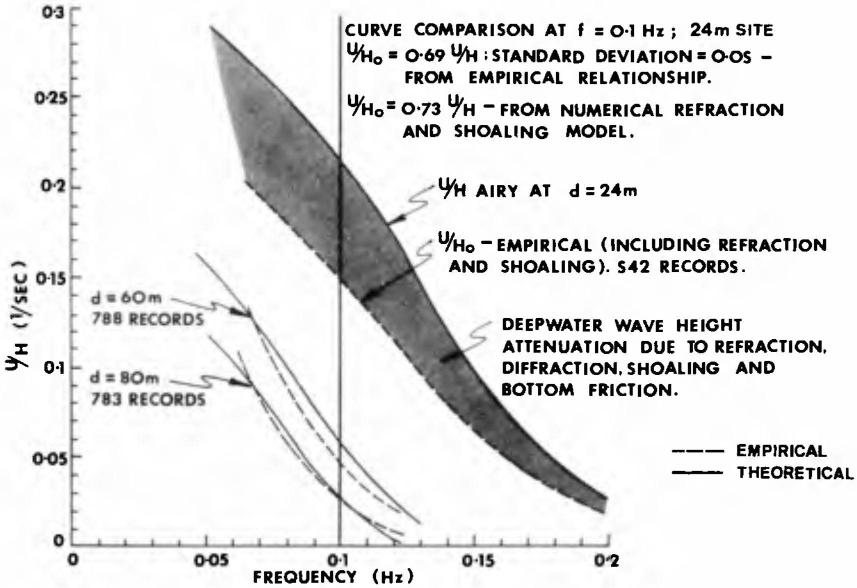

ACROSS SHELF CROSS-SPECTRAL CORRELATIONS BETWEEN DEEPWATER WAVERIDER AND CURRENT METER RECORDS

FIGURE 3

The results of the analyses showed that a reasonable approximation of wave-induced seabed current energy can be made by spectral transfer of waverider data to the seabed using monochromatic wave theories to obtain values of the velocity/wave height ratio in Equation 1. Where refraction, diffraction, shoaling and the effects of bottom friction are significant, the theoretical values of the velocity to wave height ratio may be adjusted on the basis of numerical modelling. However, where wave height attenuation is severe the application of simple numerical models may not be appropriate (Nielsen, 1984).

3.2 Characteristic Spectral Parameters for Sediment Motion

To apply the existing understanding of sediment transport processes to natural field situations it was first necessary to examine the appropriateness of characterising natural energy spectra in terms of displacement and frequency parameters. It was considered that an examination of bedform response to near-bed velocity spectra could be used to indicate and evaluate such characteristic parameters if appropriate; there being considerable data available from flume and oscillating water tunnel experiments concerned with bedform response to periodic, progressive, near-sinusoidal water movements.

Laboratory data were examined and it was found that the bedform curves of Mogridge and Kamphuis (1972) described and quantified well the existing understanding of bedform generation and degeneration under monochromatic wave conditions (Figure 4). Also, Nielsen (1984) reviewed the field data of Inman (1957) and compared them to the bedform curves of Mogridge and Kamphius. To obtain a good agreement between these data and the laboratory results it was necessary to increase Inman's calculated significant hydraulic parameters by a factor of 1.5. Inman's hydrodynamic data were based on fathometer records and that, coupled with the considerations of depth effect on surface displacement energy, is considered to have resulted in his over-estimation of near-bed velocities and displacements.

At the 80 metre site no bedform generation was observed during the 6 month deployment period. The film indicated that sheet flow rapidly followed the onset of transport. This is believed to be due to the high fines content (Table 1) and the high level of biogenic activity at the site which together produced a partly cohesive bed (Gordon and Hoffman, in prep.).

While at the 60 metre site some bedform activity was noted these bedforms were poorly developed and the resolution of the film was such that no accurate measurements of bedform size could be made (Gordon and Hoffman, in prep.).

The most reliable field data set comprised forty-three separate events for which bedform geometric data were obtained at four locations adjacent to the 24 metre site (Figure 1).

The bedform observations were taken by divers and included measurements of ripple wavelength, height, and crest orientation, assessments of ripple assymetry, general bedform configurations and whether the sand grains on the bed were active or inactive. The data

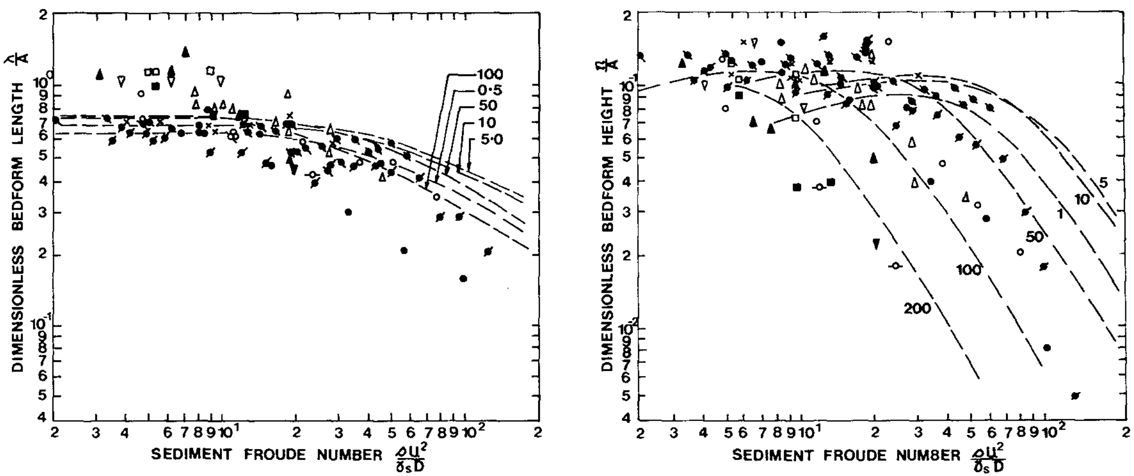

LEGEND :

symbol	$\frac{\rho D}{\delta_s T^2} \times 10^6$	symbol	$\frac{\rho D}{\delta_s T^2} \times 10^6$	symbol	$\frac{\rho D}{\delta_s T^2} \times 10^6$	symbol	$\frac{\rho D}{\delta_s T^2} \times 10^6$
●	1·0	×	8·0 – 10·0	▽	136	▼	500
● (flagged)	1·4 – 2·6	○	55	□	242	■	600
● (flagged)	3·1 – 6·5	△	94 – 116	▲	350	-○-	850

— — — Bedform height curves modified after Mogridge & Kamphuis (1972); numbers to each curve are values of $\frac{\rho D}{\delta_s T^2} \times 10^6$

COMPARISION OF DATA FROM INMAN & BOWEN (1963), KENNEDY & FALCON (1965) HORIKAWA & WATANABE (1967), CARSENS ET AL. (1969) & LOFQUIST (1980) WITH BEDFORM CURVES MODIFIED AFTER MOGRIDGE & KAMPHUIS (1972)

FIGURE 4

are summarised in Table 2 and detailed in Nielsen (1984). The ripple wavelengths were measured by placing a scaled ruler over and normal to the ripple crests. Most of the wavelength measurements over 100 mm were made to the nearest 50 mm. The accuracy of wavelength measurements is considered to be ± 25 mm for those measurements recorded to 50 mm, and ± 10 mm for measurements recorded to 10 mm. Ripple heights were measured by placing a second scale vertically and normal to the ruler across the ripple crests, measuring down to the ripple troughs. In most cases, these measurements were taken to 10 mm (or in inch, equivalent to 25 mm) and the accuracy of these measurements is considered to be ± 10mm. Ripple orientations were measured by diver compass sightings along the ripple crests. Measurements were made to magnetic north with an estimated accuracy of ± 15°. It is to be noted that the bedform patterns on the seabed where measurements were taken were not always uniform. The divers assessed the bedform distributions and took measurements where "average" bedform characteristics prevailed. The accuracies quoted above do not apply to the variations in bedform size parameters observed at the measurement sites.

The water particle velocity measurements could not necessarily be taken simultaneously with the bedform measurements. As bedform measurements were made at meter servicing times, most (70%) of the bedform measurements were made within seven hours of the velocity readings. As waverider data were generally available every six hours, bottom velocities and bedform data could be related through the waverider records, using the method for bottom transfer (section 3.1), when there were large elapsed times between the two.

As reported by Inman (1957), the sand ripples observed in this study varied widely in size, shape and duration. Some ripples were uniform with long parallel crests, others occurred in complex patterns. During some observations the ripples, while active, appeared not to change much in time, whereas during other observations the ripple bed erupted and disappeared under large wave surges only to rapidly reform following the passage of the surge. It was difficult in most cases to ascertain if the ripples measured were formed by the waves present at the time of measurement. One reason for this was that to avoid decompression procedures the divers had a limited bottom time to observe the ripple behaviour. If the ripples were active it was not necessarily clear if they were changing to a new equilibrium with the wave forces or whether they had attained a stable form. In some cases, a judgement could be made as to whether the ripples were in equilibrium with the wave climate by comparing ripple orientations to wave directions. In other cases this was not possible. In the main the divers, including the authors, were experienced investigators.

A convenient way of describing ripple geometry is by the ripple steepness η/λ. The bedform curves of Mogridge and Kamphuis indicate that there is a maximum attainable value of ripple steepness. They found that while this maximum value varied according to the specific gravity of the sand particles, for quartz sand under the range of natural field hydraulic conditions pertaining to this study, 0.16 is the maximum attainable value of steepness for wave-generated ripples (based on regular, near-sinusoidal, periodic fluid motion). This result is generally in agreement, albeit at the lower end of the

TABLE 2

REF. NO.	DATE	TIME (hrs:mins)	DEPTH (m)	λ (mm)	η (mm)	CURRENT METER (site no; tima)	WAVERIDER (I= Inshora O=Offshore;times)	COMMENTS (A=active; I=inactive; S=symmetrical; N=not in equilibrium with wave climate)
SITE 1								
1	19:6:81	12:20	23·7	350	60	1;2030	I; 0854, 1446	A, S
2	27:7:81	14:30	24·0	225	35	–	I; 1446	I, S
3	12:10:81	11:00	23·4	100	60	1;0445	I; 0845, 1445	I, S
4	12:11:81	13:15	23·0	250	50	1;0945, 1645	–	I, S
5	3:2:82	07:45	23·5	500	100	–	O;0600, 1200	A, S
6	11:3:82	14:15	23·0	500	50	1; 1550	O; 1200, 1800	A, S
7	4:5:82	10:30	23·4	250	70	1; 0750	O; 0600	I, S
8	14:9:82	10:00	24·0	250	70	1;0740	I; 0711, 1311	A, –
SITE 2								
9	23:11:79	08:30	24·5	250	20	2;1136	O; 0900	A, –
10	29:11:79	07:20	24·0	380	75	2;0630	–	A, S
11	14:12:79	14:00	24·0	450	185	2;0630, 1830	O;0828, 1426, 2030	A, –
12	14:1:80	09:30	23·9	1000	200	2;1136	O;0900, 1458	A, S
13	28:3:80	10:20	24·2	900	170	2;1536	O; 0852, 1449, 2053	I, –
14	29:4:80	10:00	24·0	1000	160	–	I; 0900, 1500	A, S
15	18:5:80	11:04	24·1	600	70	2; 1000	O; 0846, 1443	I, asymetrical
16	23:6:80	11:30	23·4	900	200	–	O; 0842, 1438	A, S
17	21:8:80	11:00	23·6	800	150	2; 1400	O;0600, 1200, 1800	A, S
18	16:9:80	10:00	24·0	600	100	–	I; 0900	I, S
19	30:10:80	10:20	24·0	700	150	–	I; 0900	A, S
20	4:12:80	10:00	23·7	400	100	2;0940	I; 0900	A, N, S
21	16:12:80	09:40	23·6	400	100	–	I; 0900	I, S
22	22:1:81	11:40	24·3	500	70	2;0605	I; 0900, 1500	A, N, S
23	3:3:81	11:00	23·5	750	150	2;1940	I; 0848, 1448	A, S
24	11:3:81	10:30	23·9	500	150	2;2045	I; 0839, 1439	A, S
25	17:6:81	13:00	23·5	600	100	2;0215	I; 2055, 0303	A, S
26	27:7:81	12:30	23·8	800	150	2;1545, 1845	I; 0854, 1446	–, –
27	19:11:81	10:30	23·5	400	80	2;2345	–	A, S
28	22:12:81	12:15	23·5	700	80	2;0845, 2245	–	A, N, –
SITE A5								
29	15:1:80	12:50	22·8	500	50	2; 1136, 1536	–	A, S
30	29:4:80	13:30	22·4	400	30	–	I; 0900, 1500	A, S
31	16:5:80	14:10	22·4	300	75	2; 0900, 1600	–	A, S
32	4:9:80	11:45	22·0	400	80	2; 0700, 1400	I; 0900, 1500	A, S
33	16:9:80	14:05	22·6	300	100	–	I; 1500	–, –
34	3:3:81	14:30	23·0	400	100	2; 1940	I; 1448	A, asymetrical
35	8:10:81	13:20	23·4	300	70	1; 0945, 1645	I; 0845, 1445	A, S
SITE B5								
36	29:2:80	11:10	24·0	250	50	2;1136	O; 0856, 1406	I, N, S
37	1:4:80	12:30	23·5	200	50	2;1136	I; 0900, 1500	I, N, S
38	29:4:80	12:30	22·8	80	30	–	I; 0900, 1500	A, S
39	16:5:80	12:15	23·0	300	70	2; 0900, 1600	–	A, S
40	4:9:80	12:15	22·5	150 & 300	25 & 50	2; 0700, 1400	I; 0900, 1500	I, N, S
41	11:3:81	13:35	22·8	200	25	2;2045	I; 1439, 2039	A, –
42	30:7:81	12:00	22·8	100	40	2;1345	I; 0854, 1446	A, S
43	8:10:81	12:30	23·0	220	25	1; 0945 1645	I; 0845, 1445	I, S

TABLE 3

REF. NO.	T_m (s)	$U_{m,100}$ (m/s)	$A_{m,100}$ (m)	$\frac{\lambda}{A}$	$\frac{\eta}{A}$	$\frac{\rho D}{\gamma_s T_m^2}$ (10^{-6})	$\frac{\rho U_{m,100}^2}{\gamma_s D}$	$\frac{\rho U_{m,0}^2}{\gamma_s D}$	$\frac{U_{m,0} D}{\nu}$	$\frac{U_{m,100}\eta}{\nu}$	DATA ASSESSMENT	ORTHOGONAL DIRECTIONS (°T.N.) WAVES	RIPPLE CRESTS
1	15·1	0·35	1·66	0·21	0·036	0·07	30·9	44·5	99	20800	P - poor	167·4	169·5
2	15·1	0·20	0·95	0·24	0·039	0·07	10·1	14·6	58	6900	F - fair	–	102·0
3	15·1	0·18	0·86	0·12	0·068	0·07	8·5	12·2	52	10900	F	154·3	147·0
4	16·9	0·26	1·42	–	–	0·05	18·0	26·0	75	13200	G - good	166·4	102·0
5	13·1	0·51	2·09	0·24	0·049	0·09	67·5	97·2	147	51200	F	–	124·5
6	10·4	0·20	0·67	0·74	0·075	0·14	10·1	14·6	58	9900	G	138·4	124·5
7	12·4	0·22	0·82	0·30	0·084	0·11	12·0	17·3	62	15000	F	145·7	127·0
8	15·1	0·22	1·03	0·24	0·067	0·07	12·0	17·3	62	15000	G	156·0	127·0
9	0·8	0·20	0·62	0·40	0·032	0·21	5·5	7·9	107	4000	F	87·0	102·0
10	9·9	0·17	0·52	0·73	0·146	0·30	3·8	5·5	89	12400	G	127·7	102·0
11	12·9	0·30	1·16	0·39	0·160	0·18	12·0	17·3	161	55000	P	112·2	–
12	12·9	0·26	1·05	0·95	0·190	0·18	9·6	13·8	143	52900	F	118·2	124·5
13	11·4	0·18	0·67	1·35	0·255	0·22	4·6	6·7	99	30900	P	95·3	132·0
14	12·4	0·35	1·35	0·74	0·118	0·19	16·4	23·6	188	55500	F	–	147·0
15	12·1	0·33	1·23	0·49	0·057	0·20	15·0	21·6	179	23100	F	114·5	222·0
16	14·2	0·50	2·15	0·42	0·093	0·14	33·6	48·4	268	99200	P	–	102·0
17	18·8	0·18	1·08	0·74	0·140	0·08	4·6	6·7	99	27300	F	102·8	147·0
18	14·4	0·25	1·14	0·53	0·088	0·14	8·5	12·2	135	24800	F	–	124·5
19	13·0	0·35	1·42	0·49	0·106	0·17	16·4	23·6	188	52100	F	120·1	147·0
20	11·2	0·20	0·69	–	–	0·24	5·5	7·9	107	19800	G	76·9	147·0
21	10·8	0·20	0·67	0·60	0·150	0·25	5·5	7·9	107	19800	G	112·0	102·0
22	13·7	0·23	0·99	–	–	0·16	7·4	10·6	125	16200	G	80·1	147·0
23	12·1	0·28	1·08	0·70	0·140	0·20	10·9	15·7	153	42200	G	78·7	102·0
24	12·1	0·30	1·14	0·44	0·132	0·20	12·0	17·3	161	44600	F	114·1	102·0
25	Naar-simultaneous hydrodynamic data not availabla										P	115·6	147·0
26	15·1	0·17	0·80	1·00	0·188	0·13	3·8	5·5	89	24800	G	111·0	124·5
27	Naar-simultanaous hydrodynamic data not available										P	106·3	147·0
28	12·9	0·17	0·67	–	–	0·18	3·8	5·5	89	13200	G	88·5	34·5
29	11·2	0·15	0·52	0·97	0·097	0·17	4·4	6·3	58	7400	F	108·9	102·0
30	13·0	0·31	1·29	0·31	0·023	0·12	19·1	27·5	121	9400	F	–	147·0
31	Hydrodynamic data outsida ranga of rafraction analysis										P	66·7	107·0
32	12·9	0·20	2·13	0·48	0·095	0·12	7·7	11·0	75	15900	F	121·5	147·0
33	Hydrodynamic data not available; dual rippla trains observed										P	–	–
34	12·9	0·30	1·20	0·33	0·083	0·12	17·2	24·8	115	29800	F	78·7	102·0
35	12·9	0·17	0·67	0·45	0·105	0·12	5·2	7·5	63	35900	G	132·1	147·0
36	Hydrodynamic data outaida ranga of refraction analysis										P	75·3	112·0
37	Badforms not in aquilibrium with wave climata										P	121·7	–
38	13·0	0·35	1·42	0·06	0·021	0·08	33·7	48·6	91	10400	P	–	102·0
39	Hydrodynamic data outsida range of refraction analysis										P	66·7	102·0
40	Badforms not in aquilibrium with wave climata										P	116·7	147·0
41	11·2	0·35	1·23	0·16	0·020	0·11	33·7	48·6	91	8800	P	114·1	102·0
42	12·9	0·45	1·83	0·06	0·022	0·09	56·0	80·7	117	17900	P	131·2	147·0
43	12·9	0·17	0·67	0·33	0·038	0·09	11·2	16·0	44	4100	G	132·1	124·5

range, with results from other studies (Nielsen, 1984).

The data on ripple steepness are presented in Figure 5. These data portray a scatter around an average value of $\eta/\lambda = 0.18$. For most of the data the maximum measured value of η/λ was 0.25. However, a few extreme values of $\eta/\lambda = 0.4$ were measured. Measurement error in part may account for the scatter portrayed. It is significant to note that the scatter reduced with increasing ripple wavelength. This tendency was observed also by Inman (1957, see his Figure 14); the higher values of η/λ reported by Inman were associated with the smaller ripple wavelength measurements. Inman also observed less scatter for data obtained from coarser sediments, a tendency also suggested in these data.

To determine the characteristic spectral parameters, the field data were plotted initially against the bedform curves of Mogridge and Kamphuis using significant hydraulic spectral parameters with Tf peak (not presented). It was found that the dimensionless wavelengths and wave heights of the field data points were considerably larger, on average by a factor of 2.15, than those of the laboratory data. The reason for the departure from the laboratory results was considered to lie in the choice of the velocity and displacement parameters used in the calculations of the data point co-ordinates. Consideration of the authors' diving observations while collecting the seabed data and the consistency with Inman's results suggested that maximum rather than significant spectral parameters would be more appropriate.

Goda (1974) showed that the ratio of maximum to significant wave height parameters has a mean value of 1.65 and a standard deviation of 0.26. He also showed that the ratio of the period parameter associated with the maximum wave to the period associated with the peak spectral

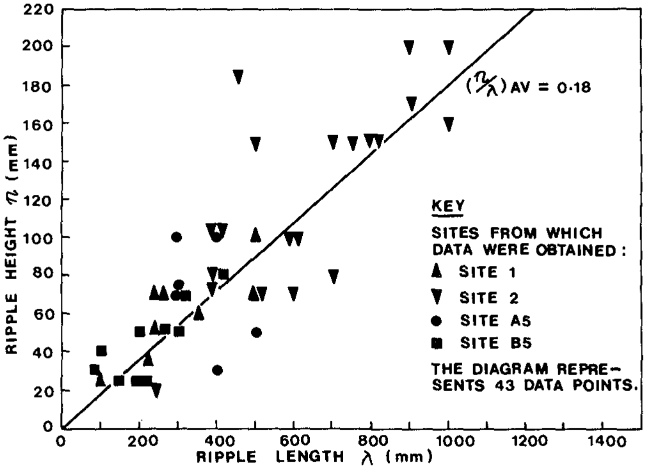

RELATIONSHIPS BETWEEN RIPPLE HEIGHTS AND RIPPLE LENGTHS

FIGURE 5

estimate lies in the range of 0.5 to 1.4. Adopting maximum spectral velocity parameters, it was found by iterative procedures that a period parameter of value 1.3 Tpeak produced a reasonable agreement between the field data and the bedform curves of Mogridge and Kamphuis (Figure 6).

The bedform investigation, therefore, suggested that maximum spectral hydraulic parameters should be used when applying existing theories based on monochromatic wave studies to shelf bed response under natural wave action; the inference being that these maximum spectral parameters should be used also for sediment entrainment and transport calculations.

3.3 Incipient Motion on a Rippled Bed

There are very little laboratory data and virtually no field data on the threshold of sediment movement on a rippled bed; most of the experimental work has been directed towards evaluating incipient motion criteria on flat beds.

Eagleson and Dean (1959) and Carstens et al. (1969) analytically considered the general condition of the threshold of motion. Their analyses were based on the hydrodynamic forces of drag and lift and the submerged weight on a typical protruding particle. Additional surface forces arising from the inertial reaction of the particles and of the fluid around the particles were not included because initial movement under wave action was observed to occur at the maximum, horizontal, near-bed velocity; that is, when acceleration in the flow is negligible.

The difficulty in applying the method, however, lies in the calibration of the constants. Where boundary layer effects become significant with oscillating flow over a duned bed, the analytical solution to the incipient motion criterion becomes very complex. It was therefore considered practical to determine empirically a threshold criterion using dimensional analysis techniques.

It was considered that for flow over a rippled bed, the important dimensionless variables were:

(1) $\frac{\rho u^2}{\gamma_s D}$ The sediment Froude number, being derived from the ratio of hydrodynamic surface forces on the sediment to the submerged weight of the sediment, which is essentially Shields parameter.

(2) $\frac{uD}{\nu}$ The particle Reynolds number upon which the sediment Froude number is dependent.

(3) $\frac{u\eta}{\nu}$ The bedform Reynolds number; a dimensionless variable introduced to take account of the effect of bedform height on bed roughness and, hence, the shear stress on the bed.

This set of dimensionless variables includes all the relevant characteristic parameters proposed by Mogridge and Kamphuis (1972) except for ρ_s, which was considered constant as the only relevant data found were observations made on quartz sand beds.

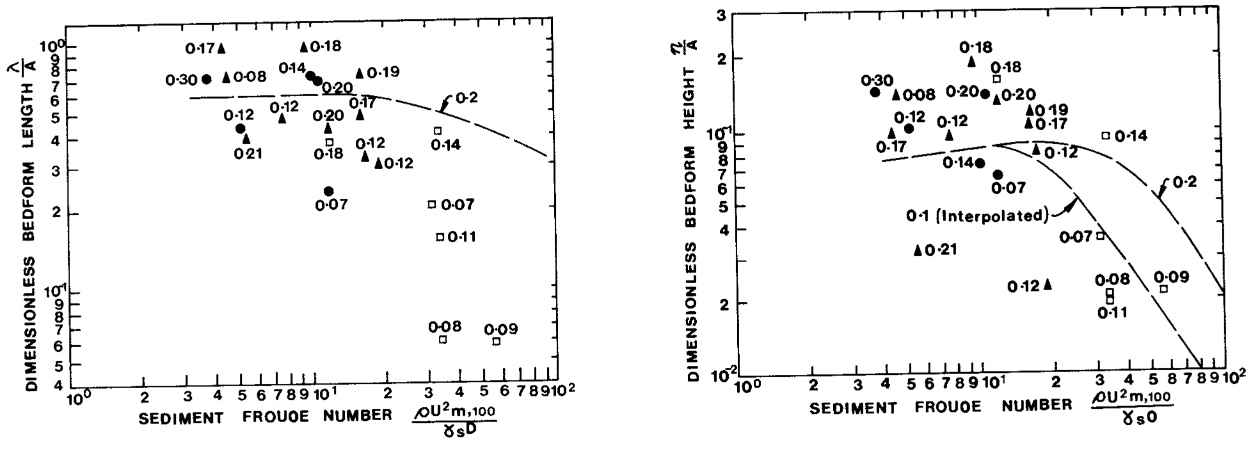

LEGEND

● GOOD
▲ FAIR
□ POOR

DATA ASSESSMENT. DATA ARE PRESENTED IN TABLES 2 AND 3.

— — — BEDFORM CURVES MODIFIED AFTER MOGRIDGE AND KAMPHUIS (1972) FOR $\frac{\rho D}{\gamma s T^2} = 0{\cdot}2 \times 10^{-6}$.

CO-ORDINATES OF FIELD DATA POINTS CALCULATED USING Um,100 AND Tmax = 1·3 Tpeak.

NUMBERS TO EACH DATA POINT ARE VALUES OF $\frac{\rho D}{\gamma s T^2} \times 10^6$. A = NEAR-BED ORBITAL DIAMETER

COMPARISON OF DIMENSIONLESS BEDFORM SIZE DATA WITH BEDFORM CURVES OF MOGRIDGE & KAMPHUIS (1972)
FIGURE 6

The field data from the 24 metre site are plotted on Figure 7 using maximum spectral velocity parameters to determine the co-ordinates of the field data points. Unfortunately, insufficient data of good quality were available to confidently define curves of constant particle Reynolds number at incipient motion. Dashed curves, therefore, have been interpolated from these data to highlight the conceptual understanding of the relationship between the sediment Froude number, particle Reynolds number and bedform Reynolds number at incipient motion and to indicate the inaccuracy in determining this relationship from these data.

These curves not only take account of those observations where the sediment was described as being at the threshold of movement, such as "just active" or "crests flipping", but also of both the "inactive" and "active" observations. For a particular curve of constant particle Reynolds number, all data lying to the upper right hand side of the curve represent a seabed condition which is either "active", with higher or lower values of particle Reynolds numbers than the curve, or "inactive" with particle Reynolds numbers higher than the value of the curve. On the lower left hand side of a particular curve, active seabed conditions occur when the particle Reynolds number is of a lower value than that of the curve, and for an inactive seabed condition that falls within this region of the graph, the particle Reynolds number may have any value.

For small bedform Reynolds numbers, that is, for small bedform heights approaching a flat bed, the interpolated bedform curves suggest values of sediment Froude number for incipient motion in the order of 100, which values are two orders of magnitude higher than would be calculated following the method of Komar and Miller (1974). However, the behaviour of the curves is not known for conditions approaching a flat bed as the hydraulic conditions near a flat bed are quite different to those of a rippled bed. For a flat bed there is no flow separation or vortex formation as observed on rippled beds, therefore, the nature of the respective boundary layers must be quite different (Carstens et al., 1969).

Additional factors considered to be important with respect to defining the location of the curves of the critical particle Reynolds numbers at incipient motion include the adopted grain size parameter and the value of bedform height. Incipient motion occurs at ripple crests. While grain size data for the ripple crests were not taken, the divers observed that the grain size on the ripple crests was different to that in the troughs. Inman (1957) and Cook and Gorsline (1972) found that the crest grain size is in the order of 0.05 mm coarser than the average grain size for sands finer than 0.5 mm. The grain size adopted will affect the values of particle Reynolds number and sediment Froude number. Bedform height data are much more difficult to measure than bedform length data, which is reflected in the wider range of scatter in bedform height data in Figure 6. In addition to bedform height being more difficult to measure, there is a greater spectral variability in bedform height than in bedform length under natural wave motion. Both of these factors will affect the determination of the proposed bedform Reynolds number and hence the accuracy to which the curves of constant particle Reynolds number defining incipient motion can be determined.

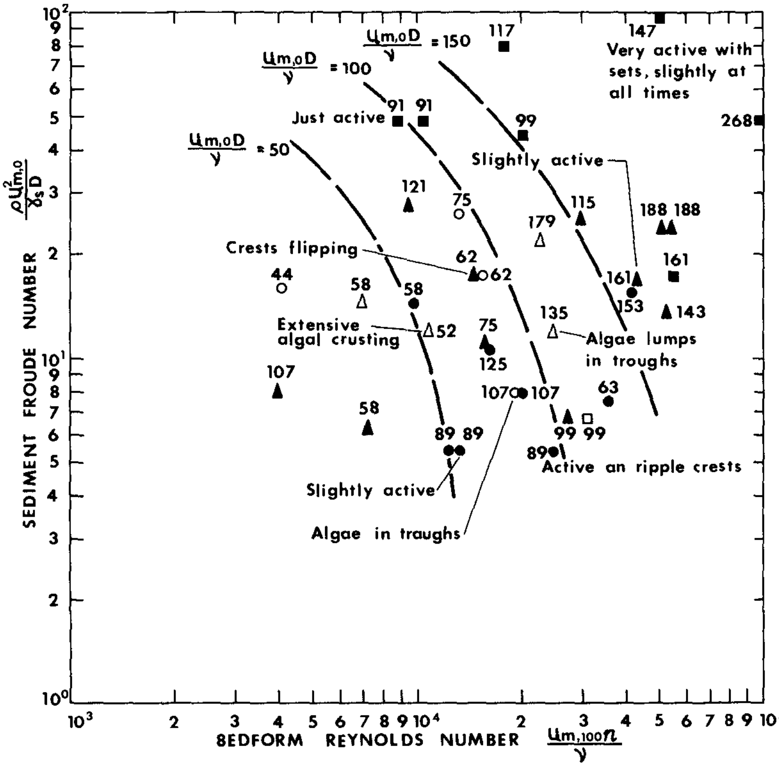

NOTES : Um,100 = Spectrol moximum, neor-bed (100 cm above), wove-induced, moximum horizontol orbitol velocity.

Um,o = 1·2 Um,100 ; the moximum velocity at dune crest (ofter Corstens et ol., 1969).

Numbers to eoch doto point ore particle Reynolds numbers.

Comments to doto points ore odditionol diver observotions not included in Tobles 2 ond 3.

LEGEND :

Inoctive	Active	
o good	● good	Assessment of doto occuracy
Δ foir	▲ fair	
□ poor	■ poor	

—— —— —— —— Interpolated curves of constont porticle Reynolds number defining incipient motion.

RELATIONSHIP BETWEEN SEDIMENT FROUDE NUMBER, PARTICLE REYNOLDS NUMBER AND BEDFORM REYNOLDS NUMBER DEFINING INCIPIENT MOTION ON RIPPLED BEDS FIGURE 7

4. CONCLUSIONS

The cross-spectral correlation analysis showed that by using an appropriate wave theory, it was possible to synthesise spectra of seabed oscillatory water particle motions with those of sea surface displacements. Further, this could be achieved at stations remote from the wave data collection site by applying suitable wave refraction, attenuation and shoaling factors obtained by monochromatic theories.

An examination of seabed response to natural wave spectra suggested that for applying monochromatic sediment entrainment and transport theories, calibrated to laboratory results, to shelf bed sediment transport studies, the appropriate characteristic spectral parameters are:

$$H_m = 1.65\ H_s;\ u_m = 1.65u_s;\ Tm = 1.3\ Tp$$

This assumed that the bedform response mechanism was indicative and therefore typical of sediment movement mechanisms including incipient motion and entrainment. That the data were limited to a single water depth, a narrow band of slight wave conditions due to diving safety provisions, limited variation in quartz sand grain sizes and the difficulty of taking precise diver measurements, dictates that in the definition of these characteristic parameters, the constants 1.65 and 1.3 be seen as preliminary figures only. Further, it must be recognised that the overall aim was to develop a method of calculating sediment movements on the Continental Shelf for engineering projects.

The incipient motion investigation indicated that incipient motion on a rippled bed occurs at considerably lower energy conditions than on a flat bed for fine to coarse sands. The criteria for incipient motion on a duned bed include both particle roughness and bedform roughness, both affecting the level of shear stress at the bed. While trends in the field data are apparent, further data are required to confidently define the relationships between the Shields parameter, particle Reynolds number and bedform Reynolds number for incipient motion on a rippled bed.

5. ACKNOWLEDGEMENTS

This paper is published with the permission of the New South Wales Public Works Department. The authors are indebted particularly to the following Departmental officers who also performed diving duties and made bedform measurements; Bandu Sena, John Hoffman, Doug Lord, Mike Nolan, Mike Geary, Bob Sneddon, Jim Lawler and Bruce Fidge.

6. REFERENCES

Carstens, M.R., Neilson, F.M. and Altinbilek, H.D. (1969). Bedforms generated in the laboratory under oscillatory flow: analytical and experimental study. TM-28, U.S. Army Corps of Eng., CERC June, 1969.

Cook, D.O. and Gorsline, D.S. (1972). Field observations of sand transport by shoaling waves. Marine Geology, 13: 31-55.

Eagleson, P.S. and Dean R.G. (1959). Wave-induced motion of bottom sediment particles. Jnl. Hydraulics Div., A.S.C.E., proc. paper 2202.

Gordon, A.D. and Hoffman, J.G. (1984). Sediment transport on the South-East Australian Continental Shelf. Proc. 19th I.C.C.E. Houston, Texas. Sept. 3-7, 1984.

Gordon, A.D. and Hoffman, J.G. (in prep). Report in preparation on sand transport processes relating to proposed seabed sewage outfall diffuser installations. N.S.W. Public Works Department, Coastal Branch.

Hoffman, J.G., Gordon, A.D., Nielsen, A.F. and Lord, D.B. (1980). Assessment of environmental impact; marine aggregate project, Broken Bay, N.S.W., New South Wales Public Works Department, Coastal Branch, Rpt. No. 80022.

Horikawa, K. and Watanabe, A. (1967). A study on sand movement due to wave action. Coast. Eng. Japan, Vol. 10, 1967. pp 39-57.

Inman, D.L. (1957). Wave generated ripples in nearshore sands. Beach Erosion Board, TM-100.

Inman, D.L. and Bowen, A.J. (1963). Flume experiments on sand transport by waves and currents. Proc. 8th Int. Conf. on Coast. Eng., Mexico City, Mexico.

Kennedy, J.F. and Falcon, M. (1960). Wave generated sediment ripples. Mass. Inst. Tech., Dept. Civil Eng. Hyd. Lab., Rpt. No. 86, August, 1965.

Komar, P.D. and Miller, M.C. (1974). Sediment threshold under oscillatory waves. Proc. 14th Coast Eng. Conf., Copenhagen, June 24-28, 1974.

Lofquist, K.E.B. (1980). Measurements of oscillatory drag on sand ripples. Proc. 17th Int. Conf. Coast. Eng., Sydney, Australia, March 23-28, 1980.

Mogridge, G.R. and Kamphuis, J.W. (1972). Experiments on bedform generation by wave action. Proc. 13th Coast. Eng. Conf., Vancouver, B.C. Canada, July 10-14, 1972.

Nielsen, A.F. (1984). Sand Ripples Under Natural Waves. M. Eng. Sc. Thesis, Univ.of New South Wales, February 1984.

Youll, P.H. (1981). Botany Bay waverider systems - ten years of records. Proc. 5th Aust. Conf. Coast & Ocean Eng., Perth, Western Aust., November 25-27, 1981.